Applied Catalysis B: Environmental 136–137 (2013) 210–217

Contents lists available at SciVerse ScienceDirect

Applied Catalysis B: Environmental

journal homepage: www.elsevier.com/locate/apcatb

# The effect of lanthanum doping on activity of Zn-Al spinel for transesterification

Qianhe Liu[a,b], Lei Wang[a], Congxin Wang[a,b], Wei Qu[a], Zhijian Tian[a,c,*], Huaijun Ma[a], Donge Wang[a], Bingchun Wang[a], Zhusheng Xu[a]

[a] Dalian National Laboratory for Clean Energy, Dalian Institute of Chemical Physics, Chinese Academy of Sciences, Dalian 116023, China
[b] University of Chinese Academy of Sciences, Beijing 100049, China
[c] State Key Laboratory of Catalysis, Dalian Institute of Chemical Physics, Chinese Academy of Sciences, Dalian 116023, China

ARTICLE INFO

*Article history:*
Received 14 October 2012
Received in revised form
10 December 2012
Accepted 26 January 2013
Available online 15 February 2013

*Keywords:*
Biodiesel
Transesterification
Lanthanum doping
Zinc aluminate
Spinel

ABSTRACT

The transesterification of soybean oil with methanol to biodiesel using lanthanum doped zinc aluminate with spinel structure as catalyst is studied. The catalyst was characterized by X-ray diffraction (XRD), $N_2$ adsorption/desorption, temperature programmed desorption of $CO_2$ ($CO_2$-TPD) and infrared spectroscopy of $CO_2$ adsorption ($CO_2$-IR). The results of $CO_2$-IR show that the basic sites of La doped zinc aluminate are surface isolated $O^{2-}$ anions and $OH^-$ groups. The results of $CO_2$-TPD show that the total amount of basic sties of the catalyst improves with the increase of the La doping amount until which is to 18.5 wt%. Doping La also enlarges the pore volume and diameter of zinc aluminate. It gets the largest pore volume (0.30 $cm^3\,g^{-1}$) and pore diameter (7.9 nm) when doped with 5.5 wt% La. Zinc aluminate doped with 5.5 wt% La (5.5% La/$ZnAl_2O_4$) exhibits the highest activity, with which the biodiesel yield exceeds 95% at 160 °C, 2.0 MPa and 0.9 $h^{-1}$. Furthermore, the transesterification reaction of about 500 h in a fixed-bed reactor was carried out over 5.5% La/$ZnAl_2O_4$ catalyst. No deactivation and leaching of catalyst components were happened on the catalyst in reaction.



## 1. Introduction

Biodiesel refers to mono alkyl esters of long chain fatty acids (FAME), which are derived from transesterification of vegetable oils or animal fats mainly [1]. Biodiesel is a clean, non-toxic and renewable fuel. It has the similar physicochemical and fuel properties to petroleum-based diesel [2]. Therefore, biodiesel can be a candidate for petroleum-based diesel. Traditionally, the transesterification reaction is carried out in a batch reactor using homogeneous alkaline catalysts (such as NaOH, KOH, NaOMe and KOMe) at 60–80 °C [3]. After the reaction, the biodiesel is separated and purified. Homogeneous alkaline in the biodiesel should be neutralized by acid solution firstly and then washed with water. Therefore, the main drawbacks of this homogeneous catalyst-based process are high costs of biodiesel production, the generation of large amounts of wastewater and the impossibility of reusing the catalyst [4]. However, the usage of heterogeneous base catalysts can resolve these problems. It realizes the low costs of biodiesel production and eliminates wastewater. More importantly, the solid base catalysts can be reused.

Generally, the solid bases reported for transesterification are inorganic solid including supported alkali metal oxides and alkaline earth metal oxides. The $Al_2O_3$ loaded with alkali metal oxides ($Li_2O$, $Na_2O$, or $K_2O$) by impregnation method showed good activity at mild reaction conditions [5–10]. Kim et al. [11] prepared a Na/NaOH/γ-$Al_2O_3$ heterogeneous base catalyst which showed almost the same activity to conventional homogeneous NaOH catalyst. Li and co-workers [12] reported that when γ-$Al_2O_3$ was loaded with KOH and K, the produced Al–O–K species resulted in an increase of the catalytic activity. However, leaching of alkali metal happened on most supported alkali metal catalysts, which resulted in the deactivations of catalysts.

Alkaline earth metal oxides were also reported as transesterification catalysts. Granados et al. [13] studied the activated CaO for transesterification. Even if the catalyst could be reused for several runs without significant deactivation, dissolution of CaO did occur. MgO was also reported as a solid base for transesterification to biodiesel, and its catalytic behavior was mostly associated with the density of basic sites [14]. Unfortunately, it was reported that the solubility of MgO in methanol was 0.130%, so MgO would leach gradually in the transesterification reaction [15]. Additionally, the basic sites of alkaline earth metal oxides have high base strength

* Corresponding author at: Dalian National Laboratory for Clean Energy, Dalian Institute of Chemical Physics, Chinese Academy of Sciences, Dalian 116023, China. Tel.: +86 411 84379151; fax: +86 411 84379151.
*E-mail address:* tianz@dicp.ac.cn (Z. Tian).

0926-3373/$ – see front matter © 2013 Elsevier B.V. All rights reserved.
http://dx.doi.org/10.1016/j.apcatb.2013.01.065

and can be poisoned by acid gas (such as $CO_2$) from ambient environment [16].

The stability of heterogeneous catalysts is very important in their industry application. In the production of biodiesel by transesterification using solid basic catalysts, the catalysts should be insoluble in methanol and oil. According to that, zinc aluminate, which is of high surface area and meso-porosity, may be a promising catalyst for transesterification. Zinc aluminate has been used as supports or components for the synthesis of methanol [17], low temperature water gas shift reaction and methanol steam reforming [17,18]. For the metal atoms, the lower electronegativity, the higher base strength of their metal oxides. The metal oxides doped with rare earth metals which have low electronegativity will show enhanced basicity. They usually exhibit good catalytic activity in the transesterification. Russbueldt and Höelderich [19] reported the preparation of 10% oxides of Pr, Nd, Sm, La, Gd, Dy, Er, or Yb on $\gamma$-$Al_2O_3$ by impregnation method. Lanthanum was also used as a dopant to enhance the activity of MgO [20], CaO [16], ZnO [21] and $ZrO_2$ [22]. Therefore, it can be expected that when zinc aluminate doped with rare earth metal, such as La, its transesterification activity will be improved.

The origin of basic sites of metal oxides has been the subject of review, and it is believed that they are generated by the surface hydroxyl groups, $M^{n+}$–$O^{2-}$ (M = metal) pairs and surface isolated $O^{2-}$ ions [23]. Usually, infrared spectroscopy of adsorbed $CO_2$ is used to determine the basic sites of solid bases. Carbon dioxide interacts with basic sites, and the kinds of basic sites are estimated from the adsorbed states of $CO_2$.

In this present work, we studied the effect of La doping on the activity of Zn-Al spinel for transesterification of soybean oil with methanol to biodiesel. The reaction conditions and the stability of the catalyst were also investigated.

## 2. Experimental

### 2.1. Catalyst preparation

Lanthanum doped zinc aluminate catalyst was prepared by calcining La–Zn–Al coprecipitation product. An aqueous solution of $Zn(NO_3)_2{\cdot}6H_2O$, $Al(NO_3)_3{\cdot}9H_2O$ and $La(NO_3)_3{\cdot}6H_2O$ was prepared, in which Zn/Al molar ratio was 1:2. Then it was titrated cocurrently with a mixture solution of NaOH and $Na_2CO_3$ at room temperature, maintaining the pH between 8.0 and 9.0. The slurry was aged for 20 h at 80 °C and then washed with de-ionized water until the pH value was 7.0. The obtained filter cake was dried at 120 °C for 12 h and then calcined in air in a muffle furnace at temperature of 700 °C for 2 h. The catalyst is denoted as $x$La/$ZnAl_2O_4$, where $x$ is the mass fraction of La. For comparison, lanthanum doped ZnO and $Al_2O_3$ were also prepared by the same method, and denoted as $x$La/ZnO and $x$La/$Al_2O_3$, respectively.

### 2.2. Catalyst characterization

X-ray diffraction patterns (XRD) were recorded on a PANalytical X'Pert PRO diffractometer using nickel-filtered Cu Kα radiation. The $N_2$ adsorption–desorption isotherms were measured at 77 K on a Quadrasorb SI physical adsorption instrument. The bulk elemental analyses were carried out on a Philips Magix601 X-ray fluorescence (XRF) analysis apparatus.

The basic properties of catalysts were determined by $CO_2$ temperature program desorption on an Autochem 2920 instrument. Prior to the adsorption of $CO_2$, the catalyst (200 mg) was pretreated in He flow (50 ml/min) at 700 °C for 2 h. After the pretreatment, the solids were then saturated by passing a $CO_2$ stream (50 ml/min) at 40 °C, followed by feeding He flow (50 ml/min) for another 2 h to remove the physically absorbed $CO_2$. Then chemisorbed $CO_2$ was desorbed by heating from 40 °C up to 750 °C at a rate of 10 °C/min in He flow (50 ml/min). The desorption process was monitored and quantified by a mass spectrometer (the base peak at $m/z$ = 44), preliminarily calibrated by the injection of pure $CO_2$ pulses.

Infrared spectra of samples were recorded on a Bruker TENSOR27 FTIR spectrometer. IR spectra of the samples in the region of structural vibrations were recorded using KBr pellets. For characterizing the structure of $CO_2$ chemisorbed on samples, self-supported wafers were used. Samples were pressed into thin wafers (35 mg), and calcined in the heating zone of a home-made IR cell at 400 °C for 30 min in vacuum. Spectra were obtained after $CO_2$ adsorption at room temperature for 30 min and sequential evacuation at room temperature, 100, 200, 300, and 400 °C. Each desorption temperature was held for 20 min. All spectra were recorded at room temperature.

### 2.3. Transesterification reaction

Transesterification reactions were carried out in a fixed-bed reactor with 6.0 g catalyst. For reactions, soybean oil and methanol were pumped into the reactor by two constant-flow pumps. The feed volume ratio of methanol to oil was 0.5–1:1 (molar ration of methanol/oil = 12–24:1, molecular weight of soybean oil = 890). The other reaction conditions were as follows: $T$ = 140–180 °C, $P$ = 1 atm–3.0 MPa and WHSV = 0.45–4.05 $h^{-1}$. The products were analyzed by using an Agilent GC-6890 chromatography. It was equipped with a cold on-column injection system, a flame ionization detector (FID) and a DB-5 capillary column (15 m × 0.32 mm × 1.0 μm) with helium as the carrier gas. For quantification purposes, the relative response factors were calculated and the method of the area normalization was used. The yield of biodiesel ($Y$) was calculated as follow [Eq. (1)]:

$$Y = X_{oil} \times S_{FAME} \times 100\% \quad (1)$$

where $X_{oil}$ is the conversion of soybean oil, $S_{FAME}$ is the selectivity of FAME.

The conversion $X_{oil}$ was calculated by using Eq. (2) [24]:

$$X_{oil} = 100\% - C_{TG} \quad (2)$$

where $C_{TG}$ is the sum concentrations of triglycerides determined by GC analysis (in %).

The selectivity $S_{FAME}$ was calculated according to Eq. (3):

$$S_{FAME} = \frac{C_{FAME}}{C_{MG} + C_{DG} + C_{FAME}} \times 100\% \quad (3)$$

where $C_{FAME}$, $C_{MG}$ and $C_{DG}$ are the concentrations of FAME, monoglycerides and diglycerides determined by GC analysis (in %).

## 3. Results and discussion

### 3.1. Structural characterization of La doped zinc aluminate

Fig. 1 shows the XRD patterns of $ZnAl_2O_4$ with different La doping amount. All samples can be ascribed to Zn-Al spinel structure. The characteristic peaks of Zn-Al spinel become weak with the increase of La doping amount, indicating that doping La can reduce the crystallinity of the catalysts. When the amount of doped La is more than 30.0 wt%, there are characteristic peaks of $La_2CO_5$. Furthermore, compared with $ZnAl_2O_4$, the characteristic peaks of La doped $ZnAl_2O_4$ shift to lower $2\theta$, which indicates La have entered into the crystal lattices of Zn-Al spinel. It will lead to the extension of Zn-Al spinel crystal lattice because the radius of $La^{3+}$ is 0.103 nm, which is much larger than the radiuses of $Al^{3+}$ (0.054 nm) and $Zn^{2+}$ (0.074 nm). The lattice parameter $a$ is raised from 8.065 nm to 8.077 nm as the La doping amount increase from 0 to 30.0 wt%

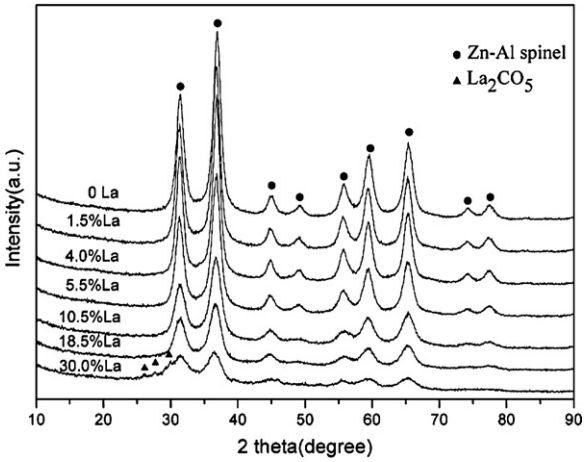


**Fig. 1.** XRD patterns of $ZnAl_2O_4$ with different amount of doped La.

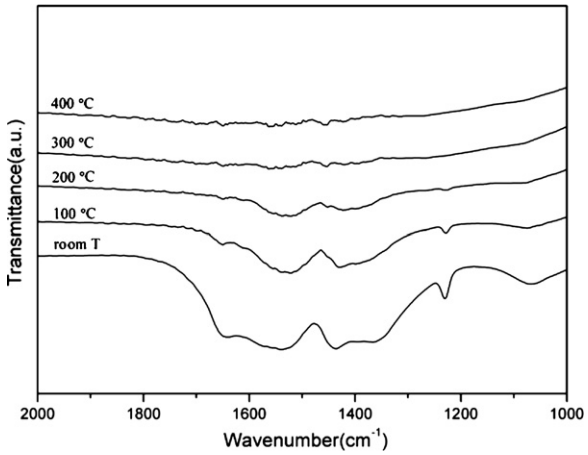


**Fig. 2.** Infrared spectra of $CO_2$ adsorbed on $ZnAl_2O_4$ upon increasing evacuation temperatures.

(Table 1). The measured atomic ratios of Al/Zn in $x$La/$ZnAl_2O_4$ samples are about 1.5 by XRF, but the XRD patterns of $x$La/$ZnAl_2O_4$ show the peaks of Zn-Al spinel only and no peaks of ZnO and $Al_2O_3$. This is not surprising, it was reported that $MgAl_2O_4$ could dissolve small amounts of MgO leading to nonstoichiometric solid solution spinels [25]. Nevertheless, superfluous ZnO might be also dissolved in the $ZnAl_2O_4$ to form nonstoichiometric Zn-Al spinel.

All $x$La/$ZnAl_2O_4$ exhibit type IV isotherms and their porosity properties are shown in Table 1. Doping La can enlarge the pore diameter and volume of zinc aluminate. The zinc aluminate doped with 5.5 wt% La has the largest pore diameter (7.9 nm) and volume (0.30 $cm^3\ g^{-1}$). More doped La results in the decrease of pore diameter and volume of zinc aluminate. This decrease may be caused by the formed $La_2CO_5$ on the surface of zinc aluminate.

### 3.2. Basicity of La doped zinc aluminate

$CO_2$ as an acidic molecular can be adsorbed on the surface of basic solids. Infrared spectra of $CO_2$ adsorption and $CO_2$ temperature program desorption are usually used to determine the basic properties of solid bases.

Different species can be formed on basic sites with diverse strengths when $CO_2$ is chemisorbed on the surface of solid bases (Scheme 1). The formation of bicarbonate species involves surface hydroxyl groups ($OH^-$, weak basic sites), whereas unidentate and bidentate carbonates are formed on surface oxygen atoms [26]. Usually, $CO_2$ is adsorbed as unidentate species on low-coordinated oxygen ions which show the strong basic strength (isolated $O^{2-}$ ions). Bidentate carbonates are formed on medium-strength basic sites ($M^{n+}$–$O^{2-}$ pairs), which require the participation of neighboring metal ions [26,27]. Bidentate carbonates can be divided into chelate and bridged bidentate carbonates. Compared to free carbonate ions, the symmetry of absorbed carbonates is decreased. The absorbed carbonate generally presents two $\nu_{CO}$ bands on either side of an IR wavenumber of 1415 $cm^{-1}$, which is the asymmetric $\nu_{CO}$ vibration of free carbonate ion ($\nu_3$) [28]. These two new vibrations are often referred to as $\nu_{3as}$ and $\nu_{3s}$ [29]. The width of the $\nu_3$-band splitting of the chemisorbed carbonate anion is denoted as $\Delta\nu_3$ ($\Delta\nu_3 = \nu_{3as} - \nu_{3s}$), which can be considered as a measure of the strength of the basic sites: the lower the splitting, the stronger the basic site [26,30]. $\Delta\nu_3$ is also used for the assignation of the species modes: 100, 300 and 400 $cm^{-1}$ for unidentate, chelate bidentate and bridged bidentate, respectively [28].

Fig. 2 shows the infrared spectra of $ZnAl_2O_4$ sample after $CO_2$ adsorption at room temperature and sequential evacuation at 100 °C, 200 °C, 300 °C and 400 °C. After the adsorption of $CO_2$ on $ZnAl_2O_4$ at room temperature, bicarbonate and unidentate carbonate anions were detected by infrared spectra in 1700–1000 $cm^{-1}$ region. That is to say, Zn-Al spinel has two kinds of basic sites, which are OH groups and isolated $O^{2-}$ ions. Bands at 1648, 1440 and 1228 $cm^{-1}$ are assigned to surface bicarbonates which were formed by interaction of $CO_2$ with surface hydroxyl groups. These three bands correspond to asymmetric stretching vibration of O–C–O, symmetric stretching vibration of O–C–O and COH blending modes, respectively [27,31]. The bands at 1542, 1361 and 1077 $cm^{-1}$ are attributed to the unidentate carbonates. Usually, unidentate carbonates formed on surface isolated $O^{2-}$ exhibits O-C symmetric stretching at about 1070 $cm^{-1}$ as well as symmetric and asymmetric O–C–O stretching modes at 1360–1400 $cm^{-1}$ and 1510–1560 $cm^{-1}$, respectively [32]. It can be found that the bicarbonate species were decomposed nearly all after sequential evacuation at 100 °C. After evacuation at 300 °C, the unidentate

**Table 1**
Nitrogen physisorption data and lattice parameters of $x$La/$ZnAl_2O_4$ and $x$La/ZnO catalysts.

| Sample | Surface area ($m^2\ g^{-1}$) | Pore diameter (nm)[a] | Pore volume ($cm^3\ g^{-1}$) | Lattice parameter (a) (nm) |
|---|---|---|---|---|
| $ZnAl_2O_4$ | 103.0 | 5.6 | 0.24 | 8.065 |
| 1.5% La/$ZnAl_2O_4$ | 87.2 | 6.6 | 0.25 | 8.070 |
| 4.0% La/$ZnAl_2O_4$ | 82.5 | 7.7 | 0.27 | 8.075 |
| 5.5% La/$ZnAl_2O_4$ | 99.8 | 7.9 | 0.30 | 8.074 |
| 10.5% La/$ZnAl_2O_4$ | 126.0 | 5.7 | 0.28 | 8.073 |
| 18.5% La/$ZnAl_2O_4$ | 119.3 | 6.6 | 0.28 | 8.077 |
| 30.0% La/$ZnAl_2O_4$ | 121.2 | 5.7 | 0.28 | 8.077 |
| ZnO | 15.7 | 27.3 | 0.06 | –[b] |
| 5.5% La/ZnO | 15.4 | 27.6 | 0.07 | – |

[a] BJH desorption average pore diameter.
[b] Not calculated.

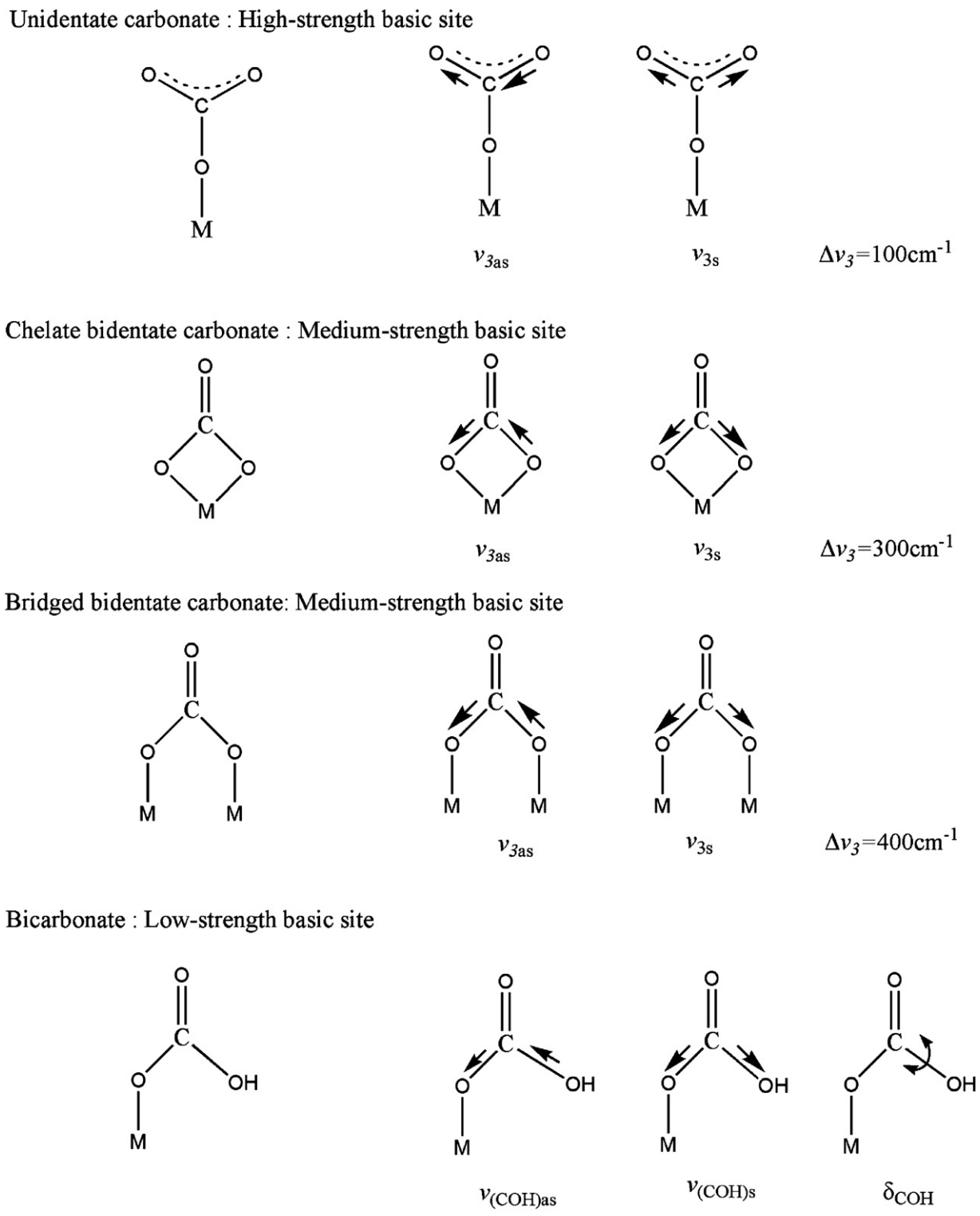


**Scheme 1.** Species formed upon $CO_2$ adsorption on metal oxides.

carbonates were removed completely from the surface of Zn-Al spinel.

The infrared spectra of $CO_2$ adsorption on 5.5% La/$ZnAl_2O_4$ shown in Fig. 3 give the similar bands to that of $ZnAl_2O_4$. However, the bands assigned to unidentate carbonate with narrower $\Delta\nu_3$ are observed after the $CO_2$ desorption at 300 °C and 400 °C. This suggests that the base-strength of isolated $O^{2-}$ ions on bare zinc aluminate can be enhanced by doping La. The results of infrared spectra of $CO_2$ adsorption suggest that both weak basic sites (surface $OH^-$ groups) and strong basic sites (surface isolated $O^{2-}$) are available on the surface of $ZnAl_2O_4$ and 5.5% La/$ZnAl_2O_4$.

Fig. 4 displays the TPD profiles of $CO_2$ on $x$La/$ZnAl_2O_4$. The quantity of evolved $CO_2$ can be denoted by the peak area of TPD curves. Overlapped peaks are observed from 40 °C to 500 °C in all samples. According to the results of $CO_2$-IR, the overlapped peak can be divided into low- and high-temperature peaks by the

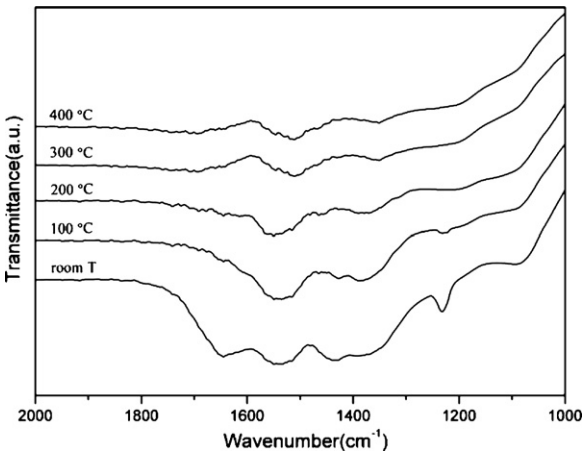


**Fig. 3.** Infrared spectra of $CO_2$ adsorbed on 5.5% La/$ZnAl_2O_4$ upon increasing evacuation temperatures.

multi-peak Gaussian fitting. Correspondingly, the low-temperature peak (peak 1) is related with weak basic sites, and the high-temperature peak (peak 2) is related with strong basic sites. It can be found that both low- and high-temperature peaks shift to higher temperature as the increase of La doping amount. The low-temperature peak shifts from 100 °C to 124 °C when the amount of La doped increases from 0 to 30.0 wt%. Although high-temperature peak shows no exact desorption temperature, it has obvious trend of shift to higher temperature with the increase of La doping amount. The low-temperature peak could be ascribed to the decomposition of bicarbonates formed on surface OH groups of *x*La/$ZnAl_2O_4$. The high-temperature peak could be ascribed to decomposition of unidentate carbonates formed on the surface isolated $O^{2-}$ anions of *x*La/$ZnAl_2O_4$. The results of $CO_2$-TPD show that doping La in Zn-Al spinel not only improves the strength of its surface isolated $O^{2-}$ basic sites, but also enhances the base-strength of surface OH groups.

The total basicity of *x*La/$ZnAl_2O_4$ is also varied with the amount of doped La (Table 2). It improves with the increase of the La doping amount until which is to 18.5 wt%. Then, it begins to decrease when the amount of La is higher than 18.5 wt%.

In order to make clear the origination of basic sites of La doped zinc aluminate, $CO_2$-TPD of *x*La/$Al_2O_3$, *x*La/ZnO and $La_2O_3$ were also studied, and the results are shown in Fig. 5. There are only weak basic sites on the surface of $Al_2O_3$ and 5.5% La/$Al_2O_3$. Compared to ZnO, 5.5% La/ZnO shows a desorption peak at 650 °C which can be

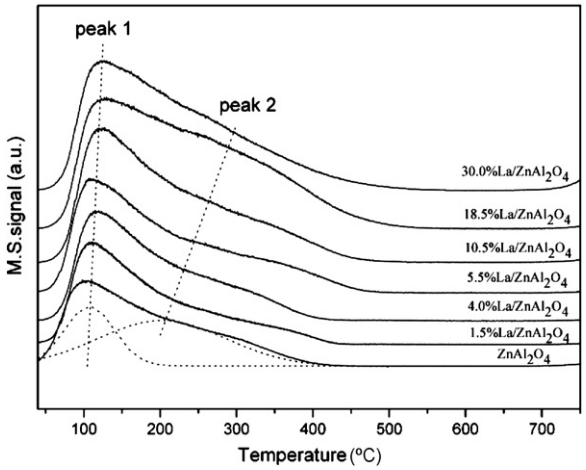


**Fig. 4.** $CO_2$-TPD profiles of *x*La/$ZnAl_2O_4$.

**Table 2**
The total basicity of *x*La/$ZnAl_2O_4$.

| Sample | Total basicity ($\mu mol_{CO_2}\ g_{cat}^{-1}$)[a] |
|---|---|
| $ZnAl_2O_4$ | 68.6 |
| 1.5% La/$ZnAl_2O_4$ | 72.9 |
| 4.0% La/$ZnAl_2O_4$ | 78.2 |
| 5.5% La/$ZnAl_2O_4$ | 98.7 |
| 10.5% La/$ZnAl_2O_4$ | 110.3 |
| 18.5% La/$ZnAl_2O_4$ | 140.5 |
| 30.0% La/$ZnAl_2O_4$ | 110.6 |

[a] Basicity is calculated according to the area of $CO_2$ desorption peaks.

attributed to the release of $CO_2$ absorbed on the surface of $La_2O_3$. The peak at 650 °C indicates that the doped La is dispersed on the surface of ZnO in the form of $La_2O_3$. This peak is not observed in *x*La/$ZnAl_2O_4$ samples (Fig. 4), which suggests the absence of $La_2O_3$ on the surface of La doped Zn-Al spinel.

In the experiments of infrared spectroscopy of $CO_2$ adsorption on $ZnAl_2O_4$ and 5.5% La/$ZnAl_2O_4$, bidentate carbonates were not detected. It indicates that the neighboring metal ions of surface oxygen ions did not participate in the chemisorption of $CO_2$. That is to say, there are no medium-strength basic sites ($M^{n+}$–$O^{2-}$ pairs) on the surface of Zn-Al spinel. However, it has the stronger basic sites, which are isolated $O^{2-}$ ions. The electronegativity of these $O^{2-}$ ions may be enhanced after the doping of La, which has lower electronegativity than Al and Zn. As the same to isolated $O^{2-}$ ions, the negative charge density carried by OH groups in La doped zinc aluminate may be also improved. Then, the basic strength of surface OH groups in Zn-Al spinel is enhanced after the doping of La. The amount of surface oxygen is also likely to be improved, which may be caused by the extension of crystal lattice of zinc aluminate after the doping of La. This improvement may lead to more total amount of basic sites in La doped Zn-Al spinel.

### 3.3. Catalytic performance

Fig. 6 displays the catalytic activity of *x*La/$ZnAl_2O_4$ in the transesterification reaction. The reactions were carried out at 160 °C, 2.0 MPa, 0.9 $h^{-1}$ and methanol/oil molar ratio of 24. Compared to bare zinc aluminate, the catalytic activity is enhanced on La doped zinc aluminate. This can be attributed to the promotion of both base-strength and total amount of basic sites caused by doping La. When the doped amount of La is 5.5 wt%, the catalyst exhibits the highest activity. Compared with 5.5% La/$ZnAl_2O_4$, the catalysts with

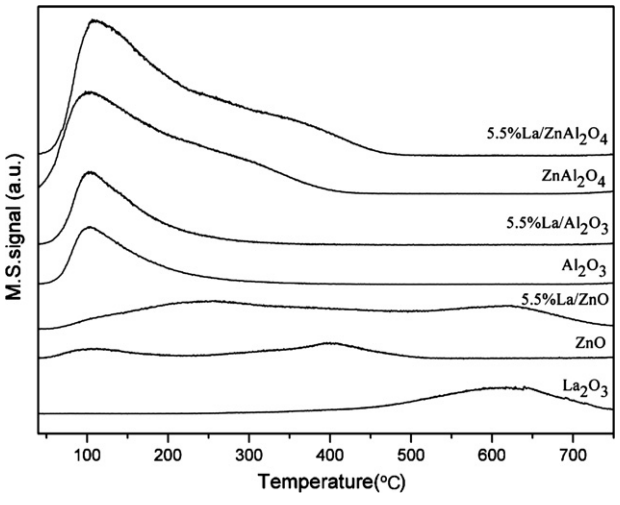


**Fig. 5.** $CO_2$-TPD profiles of $La_2O_3$, ZnO, 5.5% La/ZnO, $Al_2O_3$, 5.5% La/$Al_2O_3$, $ZnAl_2O_4$ and 5.5% La/$ZnAl_2O_4$.

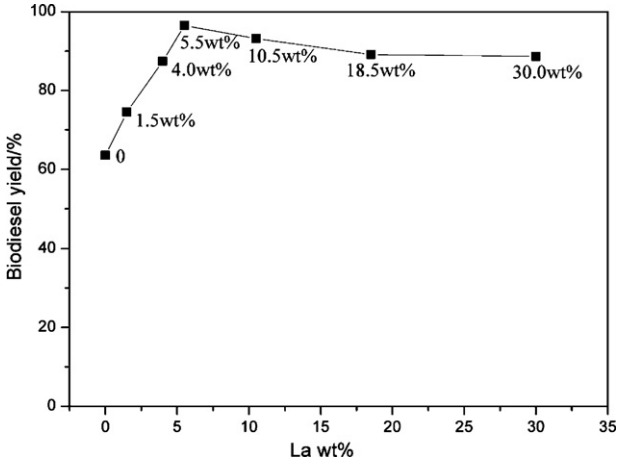


**Fig. 6.** Effect of the La doping amount in $ZnAl_2O_4$ on the biodiesel yield. Reaction conditions: WHSV, 0.9 $h^{-1}$; reaction temperature, 160 °C; reaction pressure, 2.0 MPa; the molar ratio of methanol/oil, 24. WHSV = oil weight/catalyst weight/h.

more La show lower activities even if they have higher total basicity. This can be due to their smaller pore diameters and volumes caused by the presence of $La_2CO_5$ on the surface of catalysts. The results indicate that both basicity and pore structure of La doped Zn-Al spinel play important roles in the enhancement of catalytic activity for transesterification reaction. For $x$La/$ZnAl_2O_4$ catalysts with total basicity than 98.7 $\mu mol_{CO_2}\ g_{cat}^{-1}$, the pore diameters and pore volumes may be the major factors to their activity. It was reported that a typical triglyceride molecule had a diameter of approximately 58 Å [33], so 10.5% La/$ZnAl_2O_4$, 18.5% La/$ZnAl_2O_4$ and 30.0% La/$ZnAl_2O_4$ catalysts with narrow pores and small pore volumes cannot accommodate bulk triglyceride molecules easily.

The catalytic performances of $x$La/ZnO and $x$La/$Al_2O_3$ were also tested and the results are presented in Fig. 7. For $Al_2O_3$, doping La has little effect on its activity. But for ZnO, the activity improves largely after doping with 5.5 wt% La. Considering almost no changes in pore diameter and volume of ZnO after the doping of La, the increased activity of 5.5% La/ZnO can be attributed to its enhanced base strength. Unfortunately, 5.5% La/ZnO catalyst suffers deactivity quickly.

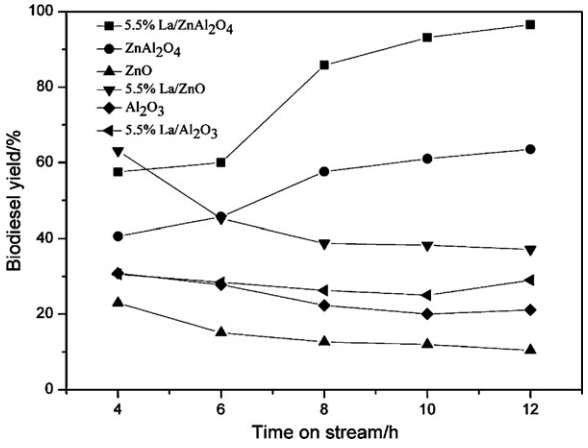


**Fig. 7.** Catalytic performances of ZnO, 5.5% La/ZnO, $Al_2O_3$, 5.5% La/$Al_2O_3$, $ZnAl_2O_4$, 5.5% La/$ZnAl_2O_4$. Reaction conditions: WHSV, 0.9 $h^{-1}$; reaction temperature, 160 °C; reaction pressure, 2.0 MPa; the molar ratio of methanol/oil, 24.

**Table 3**
Effects of reaction variables on transesterification.

| $T$ (°C) | $P$ (MPa) | $n_{methanol}/n_{oil}$[a] | WHSV ($h^{-1}$) | Biodiesel yield (%) |
|---|---|---|---|---|
| 140 | 2 | 24 | 0.9 | 84.86 |
| 150 | 2 | 24 | 0.9 | 90.74 |
| 160 | 2 | 24 | 0.9 | 96.52 |
| 160 | 1 atm | 24 | 0.9 | 60.72 |
| 160 | 1 | 24 | 0.9 | 89.43 |
| 160 | 3 | 24 | 0.9 | 96.42 |
| 160 | 2 | 24 | 0.45 | 96.94 |
| 160 | 2 | 24 | 1.35 | 93.67 |
| 160 | 2 | 24 | 1.8 | 89.46 |
| 160 | 2 | 24 | 2.25 | 84.13 |
| 160 | 2 | 24 | 2.7 | 84.37 |
| 160 | 2 | 24 | 3.15 | 72.46 |
| 160 | 2 | 24 | 3.6 | 74.34 |
| 160 | 2 | 24 | 4.05 | 59.72 |
| 170 | 2 | 24 | 0.9 | 96.87 |
| 180 | 2 | 24 | 0.9 | 97.88 |

[a] The molar ratio of methanol/oil.

### 3.4. Effects of reaction variables on transesterification

The effect of reaction temperature on biodiesel synthesis was studied on 5.5% La/$ZnAl_2O_4$. The results presented in Table 3 show that the biodiesel yield improves along with the increase of reaction temperature when it is lower than 160 °C. When the temperature is beyond 160 °C, increasing temperature has little effect on biodiesel yield. It was reported that a high temperature was favorable for biodiesel synthesis because the transesterification reaction was endothermic [34]. On the other hand, improved mixture of oil and methanol caused by high temperature can reduce the mass transfer resistance, which accelerates the transesterification reaction as well.

The effect of pressure on the performance of 5.5% La/$ZnAl_2O_4$ was also investigated. The pressure is varied in the range of 1 atm–3 MPa. As shown in Table 3, the biodiesel yield increases as the pressure increases from 1 atm to 2.0 MPa, and it gets the highest when the pressure is 2.0 MPa. Upon further increase of the pressure, the biodiesel yield remains almost unchanged. In above reaction conditions, the methanol exists mainly in gas phase, so the practical methanol/oil molar ratio in the reaction is changed with the variation of pressure.

The effect of WHSV on the performance of 5.5% La/$ZnAl_2O_4$ is also shown in Table 3, the biodiesel yield decreases with an increase of WHSV from 0.45 $h^{-1}$ to 4.05 $h^{-1}$.

### 3.5. Stability of the catalyst

The stability of the catalyst is an important factor for reducing the cost of the process. In order to verify the stability, the 5.5% La/$ZnAl_2O_4$ catalyst was evaluated in a fixed-bed reactor for about 500 h. Fig. 8 shows that the yield of biodiesel is stable around 95% in 516 h, indicating that La doped Zn-Al spinel catalyst exhibits excellent stability in the biodiesel synthesis. The XRD patterns of the fresh and used 5.5% La/$ZnAl_2O_4$ are presented in Fig. 9. From the XRD patterns, it can be found that the used catalyst still keeps the same spinel structure as the fresh catalyst. This illustrates that the crystal structure of 5.5% La/$ZnAl_2O_4$ catalyst is very stable.

It was reported that the leaching of La would result in the deactivation of $La_2O_3$ loaded catalysts [22], so we checked the components of fresh 5.5% La/$ZnAl_2O_4$ and used 5.5% La/$ZnAl_2O_4$ catalysts by XRF. Table 4 illustrates that the compositions between the fresh and the used catalysts remain almost unchanged. It is worth noting the quickly deactivation of 5.5% La/ZnO, in which the biodiesel yield decreases from 63.13% to 37.13%. Lanthanum existed in the form of $La_2O_3$ on the surface of ZnO was likely

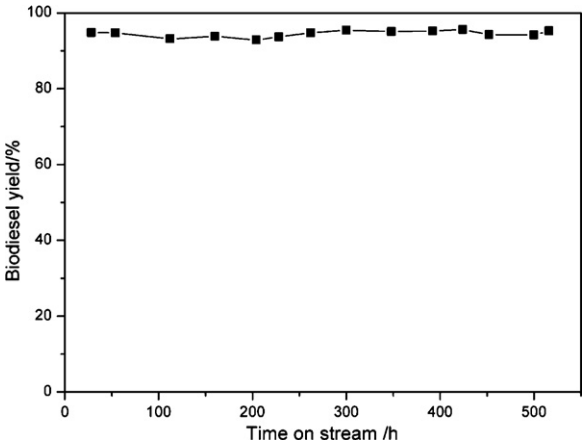


**Fig. 8.** Stability of 5.5% La/$ZnAl_2O_4$ in a fixed bed reactor. Reaction conditions: WHSV, 0.9 $h^{-1}$; reaction temperature, 180 °C; reaction pressure, 2.0 MPa; the molar ratio of methanol/oil, 12.

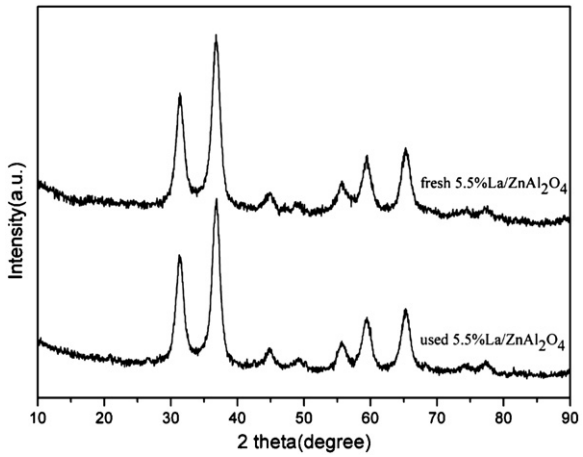


**Fig. 9.** XRD patterns of fresh 5.5% La/$ZnAl_2O_4$ and used 5.5% La/$ZnAl_2O_4$.

to dissolve in methanol, and then resulted in the deactivation of 5.5% La/ZnO catalyst. In the catalyst of La doped zinc aluminate, La locates mainly in the crystal lattices of zinc aluminate, which is insoluble in methanol. Therefore, the doped La in zinc aluminate is difficult to lose.

Yan et al. [16] reported that mixed CaO–$La_2O_3$ solid base exposed to air showed a significant decrease in catalytic activity. However, in the case of La doped zinc aluminate, exposed to air has almost no effect on its activity. IR spectra of *x*La/$ZnAl_2O_4$, *x*La/ZnO and *x*La/$Al_2O_3$ exposed to air several days are shown in Fig. 10. The bands at 1499 $cm^{-1}$ and 1396 $cm^{-1}$ are due to the vibration of $CO_3^{2-}$, which indicate the adsorption of $CO_2$ in these catalysts. These two bands are strongest in 5.5% La/ZnO, but much weaker in the samples of ZnO, 5.5% La/$ZnAl_2O_4$ and $ZnAl_2O_4$. For 5.5% La/$Al_2O_3$ and $Al_2O_3$ catalysts, these two bands almost disappear. The results suggest that 5.5% La/ZnO catalyst is more prone to adsorb the $CO_2$ in the air than other catalysts, which can be due to its surface $La_2O_3$.

**Table 4**
Amounts of metallic elements of fresh and used 5.5%La/$ZnAl_2O_4$.

| Metallic element | Relative amount (wt%) | |
|---|---|---|
| | Fresh 5.5% La/$ZnAl_2O_4$ | Used 5.5% La/$ZnAl_2O_4$ |
| Zn | 22.67 | 22.81 |
| Al | 39.99 | 39.77 |
| La | 5.7 | 5.6 |

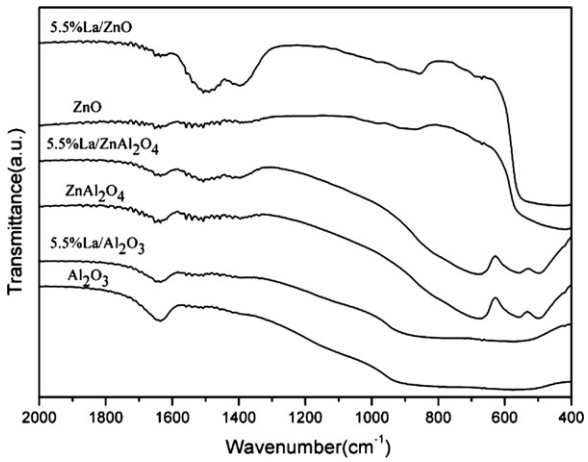


**Fig. 10.** IR spectra of 5.5% La/ZnO, ZnO, 5.5% La/$ZnAl_2O_4$, $ZnAl_2O_4$, 5.5% La/$Al_2O_3$, $Al_2O_3$.

Metal oxides with high-strength basic sites, such as alkaline earth metal oxides and rare earth oxides, are very sensitive to $CO_2$. They will lose activity when $CO_2$ is adsorbed on the surface. The basic sites of 5.5% La/$ZnAl_2O_4$ are surface isolated $O^{2-}$ and $OH^-$ groups of Zn-Al spinel, which are improved by entered $La^{3+}$. Compared to alkaline earth metal oxides and rare earth oxides, the base-strength of La doped zinc aluminate may be weaker. So La doped zinc aluminate shows less sensitive to $CO_2$, and can avoid being poisoned by $CO_2$.

In a general way, solid base catalysts often lose activity because they are prone to adsorb acid molecules (e.g. $CO_2$) from the ambient environment [35]. Moreover, dissolution of active component is difficult to avoid when solid base catalysts are applied in liquid phase reaction. Fortunately, 5.5% La/$ZnAl_2O_4$ catalyst can resolve above two questions well and shows high activity and excellent stability.

## 4. Conclusions

Lanthanum doped Zn-Al spinel catalyst calcined from La–Zn–Al coprecipitation product was studied and applied to the transesterification of soybean oil into biodiesel. Doped lanthanum is prone to enter into the lattice of Zn-Al spinel. Zn-Al spinel has weak and strong basic sites, which are enhanced in both strength and amount after the doping of La. The pore diameter of zinc aluminate is also enlarged by doping La. Both strong basicity and large pore size are beneficial to the transesterification. When the amount of doped La is 5.5 wt%, the catalyst exhibits the highest activity.

Lanthanum doped zinc aluminate can keep strong basicity because doped La in the crystal lattice of Zn-Al spinel is not prone to dissolve into methanol. Moreover, the strength of their basic sites is not strong enough to be poisoned by ambient $CO_2$. These two factors highlight the well stability of the La doped zinc aluminate. Thus La doped zinc aluminate is a promising catalyst for a green and durable biodiesel production process.

## Acknowledgement

Financial support of this work by Chinese Academy of Sciences is gratefully acknowledged.

## References

[1] L.C. Meher, D. Vidya Sagar, S.N. Naik, Renewable and Sustainable Energy Reviews 10 (2006) 248–268.
[2] C. Xua, J. Sun, B. Zhao, Q. Liu, Applied Catalysis B 99 (2010) 111–117.

[3] J.A. Melero, J. Iglesias, G. Morales, Green Chemistry 11 (2009) 1285–1308.
[4] D. Salinas, P. Araya, S. Guerrero, Applied Catalysis B 117–118 (2012) 260–267.
[5] K. Noiroy, P. Intarapong, A. Luengnaruemitchai, J.I. Samai, Renewable Energy 34 (2009) 1145–1150.
[6] A. D'Cruz, M.G. Kulkarni, L.C. Meher, A.K. Dalai, Journal of the American Oil Chemists Society 84 (2007) 937–943.
[7] X. Liu, X. Xiong, C. Liu, D. Liu, A. Wu, Q. Hu, C. Liu, Journal of the American Oil Chemists Society 87 (2010) 817–823.
[8] C.S. MacLeoda, A.P. Harvey, A.F. Lee, K. Wilson, Chemical Engineering Journal 135 (2008) 63–70.
[9] M. Verziu, M. Florea, S. Simon, V. Simon, P. Filip, V.I. Parvulescu, C. Hardacre, Journal of Catalysis 263 (2009) 56–66.
[10] T. Wan, P. Yu, S. Wang, Y. Luo, Energy and Fuels 23 (2009) 1089–1092.
[11] H.J. Kim, B.S. Kang, M.J. Kim, Y.M. Park, D.K. Kim, J.S. Lee, Catalysis Today 93 (2004) 315–320.
[12] H. Ma, S. Li, B. Wang, R. Wang, S. Tian, Journal of the American Oil Chemists Society 85 (2008) 263–270.
[13] M.L. Granados, M.D.Z. Poves, D.M. Alonso, R. Mariscal, F.C. Galisteo, R.M. Tost, J. Santamaría, J.L.G. Fierro, Applied Catalysis B 73 (2007) 317–326.
[14] M. Verziu, B. Cojocaru, J. Hu, R. Richards, C. Ciuculescu, P. Filip, V.I. Parvulescu, Green Chemistry 10 (2008) 373–381.
[15] S. Gryglewicz, Bioresource Technology 70 (1999) 249–253.
[16] S. Yan, M. Kim, S. Mohan, S.O. Salley, K.Y. Simon Ng, Applied Catalysis A 373 (2010) 104–111.
[17] M.V. Twigg, Catalyst Handbook, 2nd ed., Wolfe Pub, London, 1989.
[18] M. Turco, G. Bagnasco, U. Costantino, F. Marmottini, T. Montanari, G. Ramis, G. Busca, Journal of Catalysis 228 (2007) 43–55.
[19] B.M.E. Russbueldt, W.F. Höelderich, Journal of Catalysis 271 (2010) 290–304.
[20] N.S. Babu, R. Sree, P.S. Sai Prasad, N. Lingaiah, Energy and Fuels 22 (2008) 1965–1971.
[21] S. Yan, S.O. Salley, K.Y. Simon Ng, Applied Catalysis A 353 (2009) 203–212.
[22] H. Sun, Y. Ding, J. Duan, Q. Zhang, Z. Wang, H. Lou, X. Zheng, Bioresource Technology 101 (2010) 953–958.
[23] V. Lorenzelli, Materials Chemistry 7 (1982) 89–126.
[24] C. Wang, Z. Tian, L. Wang, R. Xu, Q. Liu, W. Qu, H. Ma, B. Wang, ChemSusChem 5 (2012) 1974–1983.
[25] P.F. Rossi, G. Busca, V. Lorenzelli, M. Waqif, O. Saur, J.C. Lavalley, Langmuir 7 (1991) 2677–2681.
[26] M. León, E. Díaz, S. Bennici, A. Vega, S. Ordóñez, A. Auroux, Industrial and Engineering Chemistry Research 49 (2010) 3663–3671.
[27] F. Prinetto, G. Ghiotti, Journal of Physical Chemistry B 104 (2000) 11117–11126.
[28] J.C. Lavalley, Catalysis Today 27 (1996) 377–401.
[29] J. Baltrusaitis, J. Schuttlefield, E. Zeitler, V.H. Grassian, Chemical Engineering Journal 170 (2011) 471–481.
[30] G. Finos, S. Collins, G. Blanco, E. del Rio, J.M. Cíes, S. Bernal, A. Bonivardi, Catalysis Today 180 (2012) 9–18.
[31] J.I. Di Cosimo, V.K. Diez, M. Xu, E. Iglesia, C.R. Apesteguia, Journal of Catalysis 178 (1998) 499–510.
[32] R. Philippt, K. Fujimoto, Journal of Physical Chemistry 96 (1992) 9035–9038.
[33] K. Jacobson, R. Gopinath, L.C. Meher, A.K. Dalai, Applied Catalysis B 85 (2008) 86–91.
[34] Z. Wen, X. Yu, S. Tu, J. Yan, E. Dahlquist, Bioresource Technology 101 (2010) 9570–9576.
[35] C.N. Satterfield, Heterogeneous Catalysis in Industrial Practice, McGraw-Hill, New York, 1991.